www.sciencemag.org/cgi/content/full/science.aag3180/DC1

Supplementary Materials for

Pyocyanin degradation by a tautomerizing demethylase inhibits *Pseudomonas aeruginosa* biofilms

Kyle C. Costa, Nathaniel R. Glasser, Stuart J. Conway, Dianne K. Newman*

*Corresponding author. Email: dkn@caltech.edu

Published 8 December 2016 on *Science* First Release
DOI: 10.1126/science.aag3180

This PDF file includes

Materials and Methods
Figs. S1 to S8
Tables S1 and S2
References

Materials and Methods

Strains, medium and growth conditions. Primers, strains and plasmids are listed in Table S2 (*31*-*33*). All expression constructs were derivatives of the IPTG inducible plasmid pET-20b(+) (Novagen). The gene for MFORT_14352 lacking the N-terminal 29 amino acids (*podA*$_{30\text{-}162}$) was PCR amplified from *Mycobacterium fortuitum* ATCC 6841 using primers listed in Table S2 and first placed into the NdeI and PstI sites of plasmid pSD5 (*34*) to verify expression of a His tag construct in a vector we used previously for *podA* expression in *Rhodococcus* sp. JVH1 (*9*). Primers encoded both a TEV protease cleavage site and a 6x-His tag on the C-terminus. Activity was observed in the *Escherichia coli* cloning strain, so we transferred the *podA*$_{30\text{-}162}$ construct to an *E. coli* expression vector for further analysis. PCR product was digested with NdeI and NotI and ligated into digested pET-20b(+) before transfer into *E. coli* BL21(DE3) cells by electroporation (*33*). Mutant proteins were generated by PCR amplifying pET-20b(+) containing *podA*$_{30\text{-}162}$ with primers encoding the relevant mutation (Table S2). Product was cut with DpnI to remove WT vector, phosphorylated with T4 polynucleotide kinase, and ligated to generate a circular mutant protein expression construct. For D72N and Y156F mutants, DNA fragments encoding the mutation were synthesized (Integrated DNA Technologies) and cloned into pET-20b(+) as for the wild type sequence. Enzymes for cloning were purchased from New England Biolabs. Constructs were transferred to *E. coli* BL21(DE3) for expression. All mutations were confirmed by Sanger sequencing (Laragen and Retrogen). When necessary, 100 μg mL^{-1} carbenicillin was included in all growth media to maintain selection for the plasmid. To measure the effect of PodA$_{30\text{-}162}$ on phenazine production in planktonically grown *P. aeruginosa*, cultures were grown overnight in 5 mL volumes of tryptic soy broth (TSB) or succinate minimal medium (arginine medium recipe from Glasser *et al*., 2014 with 40 mM sodium succinate in place of arginine) (*3*) in the presence 1 μg mL^{-1} PodA$_{30\text{-}162}$. Cells were removed by centrifugation and supernatants were analyzed by HPLC as previously described (*9*). See below for a description of biofilm growth of *P. aeruginosa* PA14.

To induce protein expression, an overnight culture was inoculated 1/1000 in Terrific Broth (BD Difco). Cultures were grown in baffled Erlenmeyer flasks (1 L culture per 3 L flask) at 37 °C with 150 rpm agitation in a shaking incubator (Innova 44 shaking incubator, New Brunswick). After 3-4 hours, the temperature was changed to 16 °C and cultures were induced with 50 μM (final concentration) IPTG and left to incubate overnight. Cells were then pelleted by centrifugation, flash frozen in liquid N_2, and stored at −80 °C for up to 1 month before protein purification.

Generation and analysis of phenazines. Pyocyanin (PYO) was purified directly from cultures of *P. aeruginosa* PA14 grown on succinate minimal medium using a previously established protocol (*31*). Briefly, culture supernatants were first extracted with 0.4 volume dichloromethane (DCM). DCM extracts were treated 1:1 with 0.01 M HCl to acidify PYO and extract it back into the aqueous phase. Finally, 1 M NaOH was added to pH7, and PYO was extracted back into DCM and dried in vacuo. This crude preparation was used for routine analysis of FPLC fractions for activity. To further purify PYO, extracts were dried and purified by reverse phase HPLC as described (*26, 31*). 1-

hydroxy-phenazine (1-OH-PHZ) was manufactured by TCI America. Phenazine-1-carboxylic acid (PCA) and phenazine-1-carboxamide (PCN) standards were purchased from Princeton Biomolecular Research, Inc. Phenazines from culture supernatants were analyzed and measured by HPLC as described previously (*6, 9*).

Protein extraction and purification. Frozen cell pellets were thawed at room temperature and suspended in 25 mL wash buffer (200 mM KCl, 20 mM imidazole, Tris, pH 7.6). Cell suspensions were homogenized in an Emulsiflex device (Avestin). Cell debris was removed by centrifugation (Avanti J-25 centrifuge, J-series JA-25.50 rotor, Beckman-Coulter) at 50,000 xg and supernatant was applied to a nickel GE Healthcare HisTrap HP 5 mL nickel column on a GE Healthcare ÄKTAxpress FPLC. All protein purification steps were carried out at room temperature. The column with bound protein was washed with wash buffer until the UV (280 nm) trace stabilized below 20 mAU. Proteins were eluted across a gradient of 20-500 mM imidazole applied over 10 column volumes. PYO demethylase activity generally eluted around 300 mM imidazole. Eluted protein was concentrated to ~3 mL (Amicon Ultra-15 centrifugal filters, Ultracel 3K MWCO) and treated overnight with 1% wt/wt TEV protease (*35*) while dialyzing (Spectra/Por Biotech Dialysis membrane, MWCO: 3.5-5 kD) into buffer containing 200 mM KCl and 20 mM Tris, pH7.6 at 4 C. Samples were run back through the nickel column and PYO demethylase activity was collected in the flow through. Protein was concentrated to 250-500 µL (Amicon Ultra – 0.5 mL centrifugal filters, Ultracel – 3K MWCO) and loaded on a GE Healthcare HiLoad 16/60 Superdex 200 prep grade gel filtration column and run at 1 mL min^{-1} with gel filtration buffer (100 mM $CaCl_2$, 20 mM Tris, pH 7.6). $CaCl_2$ in the buffer was necessary for maximal $PodA_{30\text{-}162}$ activity. Activity eluted after ~83 mL. For applications requiring highly purified $PodA_{30\text{-}162}$ (e.g., crystallography), an acid precipitation step (400 mM phosphate/citrate, pH 4.2) was added either before or after gel filtration chromatography to precipitate trace contaminants that were not apparent by SDS-PAGE. PYO demethylase activity remained in the supernatant. For acid precipitation, sample was dialyzed into 20 mM Tris, pH 7.6 between steps to avoid mixing $CaCl_2$ and phosphate buffers. Purified $PodA_{30\text{-}162}$ was dialyzed into 20 mM Tris, pH7.6 and stored at 4 °C; protein remained stable with no apparent loss of activity for as long as tested (up to 4 months). To determine the approximate molecular weight of purified proteins, the elution peak was compared to Bio-Rad gel filtration standards run across the same column with gel filtration buffer. Mutant proteins were purified on the same day as wild type and fractions where activity was seen in wild type were also collected for mutant preparations. Protein quantification was carried out by Bradford assay (*36*) (Quick Start 1x Bradford Dye Reagent, Bio-Rad) using pre-diluted Bovine Serum Albumin standards (Thermo Scientific) to establish a standard curve. A purification from 6 liters of culture typically yielded 1-2 mg protein. Purified proteins were routinely subject to SDS-PAGE using 4-20% Mini-PROTEAN TGX precast protein gels (Bio-Rad) and stained with Coomassie Blue. All protein preparations were colorless indicating that flavins were not present in the purified protein.

Enzyme activity and analysis. PYO demethylation by $PodA_{30\text{-}162}$ was first determined by HPLC analysis as described previously (*6, 9*). To detect formaldehyde evolution, 150

nM protein was mixed with 50 μM PYO in 1 mL of 20 mM Tris pH 7.6 amended with 200 μL Nash reagent (2 M ammonium acetate, 50 mM acetic acid, 20 mM acetylacetone) and incubated at 55 °C until the reaction proceeded to completion (*37, 38*). The products were determined by HPLC using the same method as used for phenazine quantification. To monitor the formation of reduced phenazine, protein and 50 μM PYO were placed into an anaerobic chamber (Coy Laboratory Products) under an atmosphere of H_2/N_2 (5:95) and left overnight before allowing the reaction to proceed. To generate reduced PYO and 1-OH-PHZ, 50 μM were mixed with 1 mM sodium dithionite. The formation of reduced phenazine products was assayed visually under UV illumination (*39*). A BioTek Synergy 4 microplate reader (BioTek) plate reader in the anaerobic chamber was used to measure the emission spectrum of products with excitation at 250 nm.

To determine the activity of $PodA_{30\text{-}162}$ in the presence of glycerol, salts, or varying pH, 30 nM protein was suspended in 500 μL buffer, 40 μM PYO was mixed with 2x solution containing the buffer of interest (500 μL), and solutions were preheated to 30 C. For pH range measurements, the following buffers were used (40 mM, adjusted with KOH): acetic acid, pH 4.9; MES, pH 5.4 and 5.7; HEPES, pH 6.1; Tris, pH 6.9 and 7.5; Bicine, pH 7.8, 8.3 and 8.7; CHES, pH 9.4. To measure reaction rates, cuvettes containing the 2x PYO solution were placed in a Evolution 260Bio UV-Vis spectrophotometer (Thermo Scientific) and 500 μL of 30 nM protein was added at time 0 (15 nM protein and 20 μM PYO, final concentration). Reaction progress was monitored by measuring absorbance at 313 nm (*40*) every 0.5 seconds for 5 minutes. To measure kinetic parameters (k_{cat}, K_m) 15 nM protein was used in a reaction buffer of Bicine, pH 7.8; reactions were monitored as before with measurements every 0.2 seconds. The rate from the first 10 seconds of the reaction was used for the determination of kinetic parameters. Kinetic parameters were calculated in Microsoft Excel using the Solver plug-in and fitting data to ideal Michaelis-Menton plots with non-linear regression of experimental data (*41*). For measurements of the rate of methoxy-PMS demethylation, 300 nM protein was used and methoxy-PMS loss from the reaction mixture was monitored at 500 nm wavelength. methoxy-PMS was purchased from TCI America. For assays with mutant proteins, 60 nM protein was used. The stimulatory effects of flavin or 2-oxoglutarate addition was determined by adding 25 μM flavin or 2-oxoglutarate to 20 μM PYO and 15 nM $PodA_{30\text{-}162}$ and monitoring the reaction.

Experiments testing alternative substrates were carried out using in 1 mL reaction volumes containing 20 mM Tris (pH 7.6) and 50 μg mL^{-1} $PodA_{30\text{-}162}$. Alternative substrates tested were 10-methylphenothiazine (AlfaAesar), phenazine methosulfate (AlfaAesar), methoxyphenazine methosulfate (TCI America), and 4-keto-N-ethylphenazine. 4-keto-N-ethylphenazine was synthesized from phenazine ethosulfate (Sigma-Aldrich) by incubating under fluorescent light overnight followed by purification by HPLC as described (*6, 42*). As phenazine methosulfate is light sensitive and spontaneously converts to PYO in the presence of light, all reactions were carried out in the dark, and activity was assessed by end point analysis by HPLC after 4 hours (*9*).

Protein crystallography, X-ray diffraction and analysis. Crystallization screens were performed with the JCSG+ screen (Molecular Dimensions) using vapor diffusion in

sitting drop format with assistance from the California Institute of Technology Molecular Observatory. A Crystal Gryphon liquid-handling robot (Art Robins) was used to mix 0.2 µL of screen solution with 0.2 µL of protein solution (5 mg mL^{-1} in 20 mM Tris, pH 7.6 amended with 200 µM 1-OH-PHZ in DMSO (1% final concentration)). Crystals formed in JCSG+ conditions C1, C6, and D12 after 3 days at 20 °C. Varying the salt and polymer concentrations in a 24-well plate showed that JSCG+ condition C1 gave robust crystal growth in vapor diffusion sitting drop format using 2 µL drops in Micro-Bridges (Hampton Research). Protein (5 mg mL^{-1}) was mixed with mother liquor (1µL:1µL) composed of 20% w/v PEG 8000, 200 mM NaCl, 200 µM 1-OH-PHZ, 1% DMSO, and 100 mM sodium phosphate dibasic/citric acid, pH 4.2. Crystals generally formed within 3 days at 20 °C and were rod shaped with typical dimensions of 50 x 50 x 100 µm. Crystals were equilibrated into a cryoprotectant solution (12% w/v PEG 8000, 20% w/v PEG 300, 100 mM NaCl, 100 µM 1-OH-PHZ, 0.5% DMSO, and 50 mM sodium phosphate dibasic/citric acid, pH 4.2) by gradually replacing the sitting drop solution with cryoprotectant solution over the span of 10–15 minutes. Crystals were then mounted in a nylon loop and flash frozen in liquid nitrogen.

Data collection was performed at 100 K at the Stanford Synchrotron Radiation Lightsource (SSRL) beamline 12-2 equipped with a PILATUS 6M Pixel Array Detector. X-ray diffraction data were collected at 12,000 eV with a beamstop distance of 32.7 mm and a detector distance of 280 nm. Images were collected every 0.15° for a full 360° of rotation around a single axis (generating a total of 2400 images). For well-diffracting crystals, an additional dataset was collected at 7,000 eV to capture the anomalous signal from sulfur and calcium. Diffraction images were integrated and scaled using the XDS package (*43*). To ensure maximum data completion, the two highest quality datasets were combined using XSCALE and further processed using POINTLESS, AIMLESS and CTRUNCATE in the CCP4 software suite (*44-48*). The structure was solved by molecular replacement in PHASER (*49*) using a search model derived from a structural prediction by Robetta (*14-16*) with disordered loops trimmed in Coot (*50*). A preliminary model was constructed using phenix.AutoBuild (*51*) and refined using phenix.refine (*52, 53*) and model building in Coot to yield a model with R_{free} = 0.22. LigandFit (*54, 55*) analysis in PHENIX (*56*) was used to model 1-OH-PHZ into the active site of $PodA_{30\text{-}162}$ with refinement restraints generated using elBOW (simple optimization method) (*57*). The model was modified in Coot to trim side chains with poor electron density coverage. A highly coordinated water molecule was identified by phenix.refine as a potential calcium atom, presumably originating from the inclusion of 100 mM $CaCl_2$ during the final protein purification step. Analysis of the anomalous difference map from a low-energy dataset supported this identification (Fig. S5) and so the corresponding water molecules were replaced with calcium atoms and metal-coordination restraints were generated with phenix.metal_coordination via ReadySet!. The final rounds of refinement were performed using TLS groups (*58*) generated by phenix.refine and hydrogen atoms set in their riding positions to yield a final model of R_{free} = 0.195. Figures were rendered with PYMOL version 1.7.2.1, Schrödinger, LLC.

Biofilm experiments. For all experiments involving inactivated PodA, either the E154A mutant or $PodA_{30\text{-}162}$ that was subjected to a 1 hour treatment at 98° C was used. To test

the ability of $PodA_{30-162}$ to degrade PYO in the presence of DNA, genomic DNA (gDNA) from *P. aeruginosa* PA14 was used in modified versions of previously described assays (*59*). For experiments using DNA pellets, 0.5 mg of gDNA was pelleted in the presence of 300 mM sodium acetate, pH 5.2 and 70% ethanol. Pellets were washed with 70% ethanol and dried. 200 µL of 800 µM PYO was added to the gDNA pellet without mixing and left to sit at room temperature for 6 hours to allow for diffusion of PYO into the gDNA pellet. The pellet was washed once with 70% EtOH, and submerged in a solution containing 10 mM Tris, pH 7.0 and 40% isopropanol. The pellet remained blue, consistent with an association of PYO with DNA. $PodA_{30-162}$ was added to the isopropanol solution to a final concentration of 2 µg mL^{-1} and left to sit for 3 hours to allow for the reaction to proceed. Tubes were imaged before and after $PodA_{30-162}$ treatment. For experiments using solubilized gDNA, a 400 µg mL^{-1} solution of gDNA was mixed with PYO and allowed to equilibrate for 6 hours. The PYO gDNA mixture was amended with 1 µg mL^{-1} $PodA_{30-162}$ and loss of PYO was monitored on a BioTek Synergy 4 microplate reader (BioTek) plate reader at 690 nm. Standards were included to quantify PYO loss over time.

To assess biofilm formation in the presence of $PodA_{30-162}$, biofilms were grown in Nunc Lab-Tek chambered coverglass slides (8-well, 0.8 cm^2 area, supplier #155411) using a modified protocol (*22*). PA14 was inoculated into succinate minimal medium and grown overnight to stationary phase. Cells were resuspended in fresh medium and diluted to a starting OD_{500} of 0.5 in succinate minimal medium. $PodA_{30-162}$ (2 µg mL^{-1}, final concentration) or DNase (20 µg mL^{-1}) (*22*) was added and 250 µL was added to each well of the 8-well chambered coverglass. Cultures were grown for 5 hours at 37 °C and 100 rpm (Innova 44 shaking incubator, New Brunswick) in a humidified chamber. After incubation, liquid was removed from each well by drawing with a pipet tip placed in the corner of each well and chambers were washed twice with 400 µL of biofilm wash (Tris buffer, pH 7.6 and 100 mM NaCl) to remove planktonic and loosely bound cells. Attached biomass was stained by adding 450 µL biofilm wash containing 10 µg mL^{-1} DAPI (4',6-diamidino-2-phenylindole) (Santa Cruz Biotechnology). Surface associated biomass was imaged on a Leica TCS SPE confocal microscope with a ACS APO 40x/1.15 oil immersion objective. A 405 nm solid-state laser was used for excitation, and data was collected from 420-500 nm. Images were collected from the same relative position in each well along the mid-point of the outer edge on the opposite edge from where the washing pipet was placed. Images were collected as 10 µm Z-stacks (10 slices) to image the biofilm in its entirety over a surface area of 40,000 $µm^2$. All Z-stacks were collected in 8-bit mode with 1024x1024 scan format and a line averaging of 2. A sum intensity projection was produced from each Z-stack using ImageJ software (*60*). Images were then thresholded to include pixels with a maximum intensity value >0.15x the maximum possible intensity, and thresholded images were used to determine surface coverage of each biofilm. Data were collected from 12 biological replicates.

Biofilm aggregate experiments. To test the effect of oxygen limitation in the presence of $PodA_{30-162}$, biofilm aggregates were grown embedded in 0.5% noble agar blocks containing succinate minimal medium. Cultures were grown overnight to stationary phase in LB, washed once with succinate minimal medium, and resuspended to OD_{600}

1.0. Samples were diluted 1:100 in agar at 44°C and 175 µL was transferred to Nunc Lab-Tek chambered coverglass slides (8-well, 0.7 cm^2 area, supplier #155409). After the agar solidified, aggregates were grown for 22 hours in a humidified chamber at 37°C before $PodA_{30\text{-}162}$ (2 µg mL^{-1}, final concentration) was added to the top of the agar for an additional 5 hours at 37°C. After treatment, 1 µL of stain from ThermoFisher LIVE/DEAD BacLight Bacterial Viability Kit in 50 µL ddH_2O was added to the top of the agar for 12 minutes before microscopic analysis. SYTO-9 from the LIVE/DEAD stain kit was used in place of DAPI to minimize background fluorescence. Biomass was imaged with a Leica TCS SPE confocal microscope with a ACS APO 10x/0.30 objective. A 488 nm solid-state laser was used for excitation, and data was collected from 510-550 nm. Images were collected across a 500 µm Z-stack with a 10 µm step size. All Z-stacks were collected in 8-bit mode with 512x512 scan format and a line averaging of 2. Biomass was quantified in ImageJ software (*60*) by identifying the Z-slice with the highest average fluorescent intensity (generally ~200 µm below the agar surface), and setting the pixel threshold using the default ImageJ thresholding parameters at the Z-slice equivalent to the 100 µm depth. The number of particles in each slice of the Z-stack was determined using this threshold value and counting particles >10 μm^2 in area. To compare biofilm aggregate biomass from different experiments, all Z-stacks were normalized by depth so that the Z-slice with the highest average staining intensity was considered the mid-point of the 3D reconstruction. This processing allowed for comparison of datasets collected on different days with slightly different staining intensities and different Z-plane starting coordinates. Particle numbers for each slice were averaged between independent experiments and plotted against depth to quantify biofilm aggregates. Only experiments with between 400 and 600 aggregates at the plane of peak stain intensity were used for averaging and statistical analysis; this ensured equivalent biomass was present in each experiment.

Oxygen diffusion modeling. To model oxygen diffusion into agar blocks embedded with *P. aeruginosa* aggregates, we utilized the oxygen diffusion model from (*29*). Cell numbers were estimated by determining the average number of aggregates present and calculating the average volume of a given particle with the ImageJ 3D-object counter plug-in (*61*). Given these values, average cell number per mL was estimated by dividing the volume of total detected biofilm aggregates by the average volume of a *P. aeruginosa* cell (*62*) yielding a cell density estimate of 5×10^8. This cell density value is consistent with the overnight growth of *P. aeruginosa* in succinate minimal medium. Oxygen diffusion was modeled using this value and 2-fold higher and lower densities to encompass a plausible range.

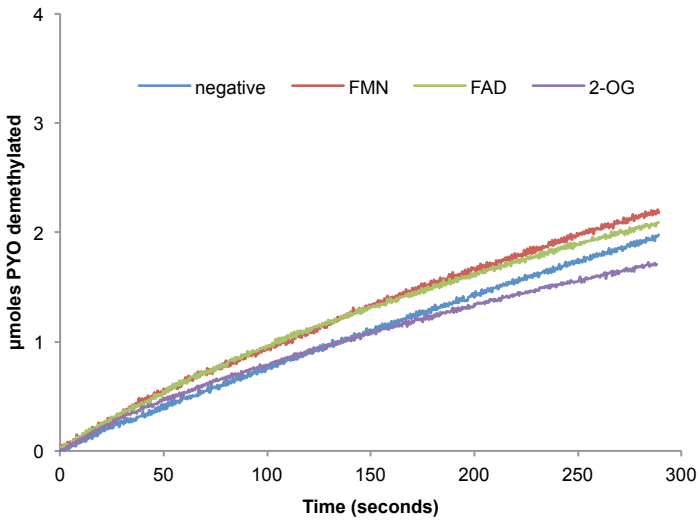

Fig. S1.

$PodA_{30\text{-}162}$ activity is not stimulated by the presence of flavins or 2-oxoglutarate (25 µM) in a reaction containing 15 nM $PodA_{30\text{-}162}$. Flavins are known cofactors for many demethylases; whereas, several others can utilize 2-oxoglutarate as an electron acceptor.

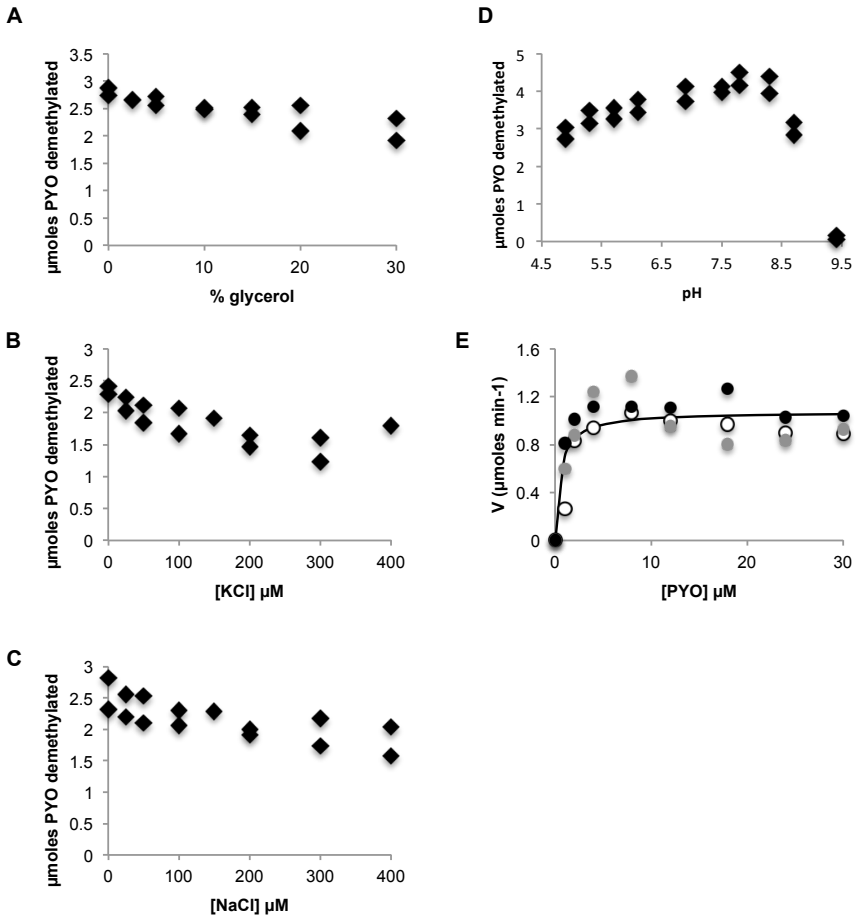

Fig. S2

$PodA_{30\text{-}162}$ activity is minimally inhibited by the presence of glycerol (**A**) or salt (**B,C**). (**D**) PodA is active over a wide pH range, but loses activity at pH above ~9. Data are from duplicate measurements and data was collected for 5 minutes in a reaction mixture containing 20 µM PYO and 15 nM $PodA_{30\text{-}162}$. (**E**) Analysis of $PodA_{30\text{-}162}$ reaction rate, V, across a range of PYO concentrations in a reaction containing 15 nM $PodA_{30\text{-}162}$. Reaction rates are from data collected during the first 10 seconds after enzyme addition. The detection limit of PYO was 0.5 µM; therefore, PYO concentrations below the K_m of the enzyme were not tested. However, based on the shape of the curve of a best fit to an ideal Michaelis-Menton plot, the apparent K_m is below 1 µM. Data are from three independent protein preparations. Each color represents data from a different protein preparation.

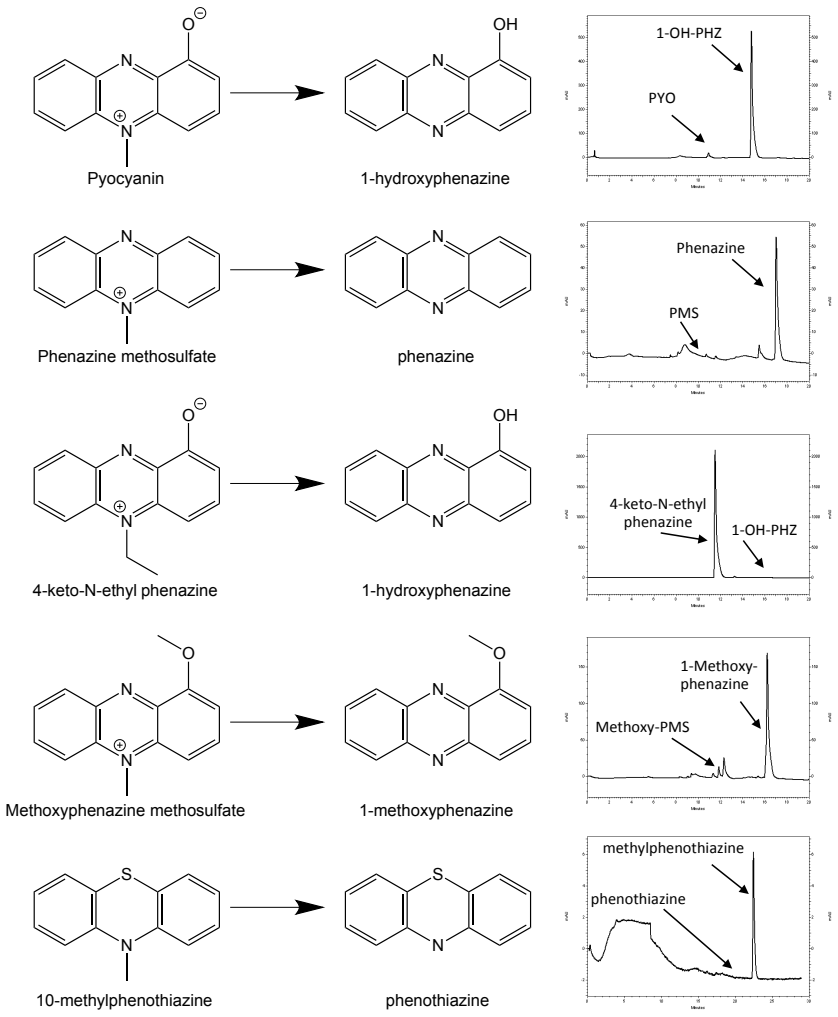

Fig. S3

Alternative substrate utilization by PodA. Methylated substrates and their predicted demethylated products are shown. Mixtures were analyzed by HPLC (right graphs) after 4 hours to determine the resulting products of each reaction. Standards for each product were run to determine retention times (indicated for each molecule with arrows). Only *N*-methylated phenazines were altered by incubation with $PodA_{30\text{-}162}$. 4-keto-N-ethylphenazine and 10-methylphenothiazine were not demethylated or de-ethylated. PMS, phenazine methosulfate.

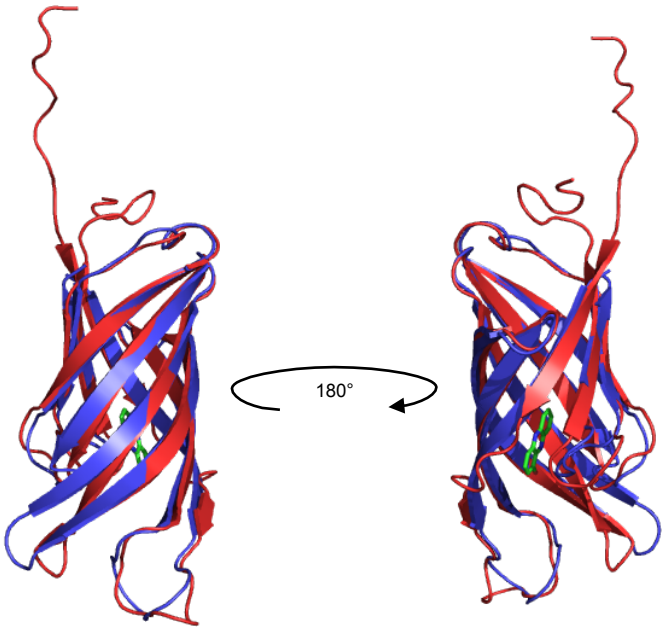

Fig. S4

Overlay of the Robetta structure prediction model (red) with the initial, solved structure of $PodA_{30\text{-}162}$ (R_{free} = 0.22 structure described in the methods) (blue). While $PodA_{30\text{-}162}$ crystallized as a trimer in the asymmetric unit, only the A chain monomer is shown here. RMSD of the C-alpha backbone: 2.23 Å vs. Robetta prediction. A version of the Robetta prediction model with trimmed loops was used to as the search model for molecular replacement (RMSD: 2.11). The N and C terminal extensions on the Robetta prediction were not resolved in the electron density of the solved structure.

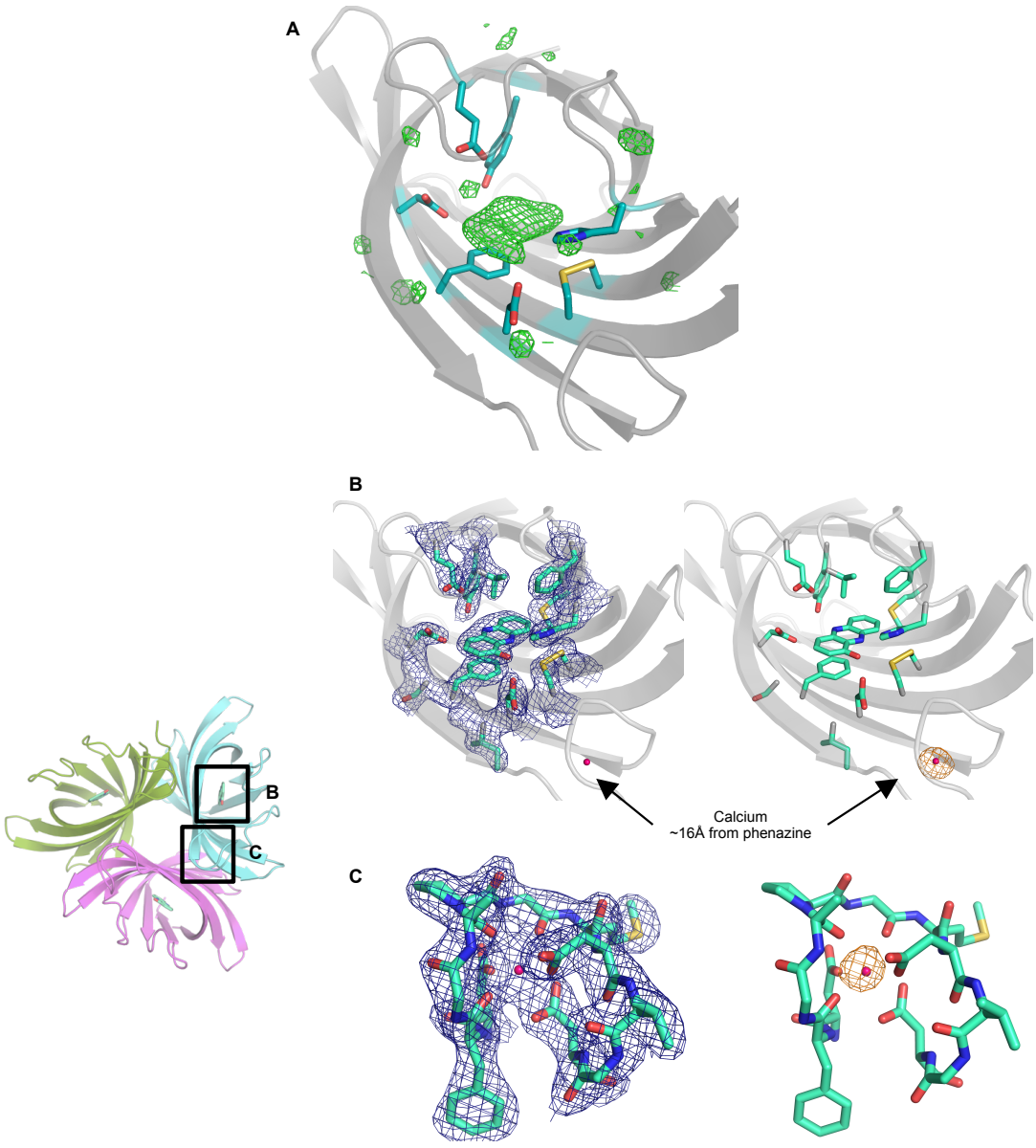

Fig. S5

Electron density maps of the PodA active site and coordinated calcium ion. (**A**) Fo-Fc map of the missing density for 1-OH-PHZ before ligand modeling and refinement (contoured at 3.0 sigma). Only the density within 5 Å of the active site residues is shown to highlight the missing ligand density. (**B**) Zoomed in view of the density around select residues in the active site (2Fo-Fc map, blue – contoured at 1.0 sigma). The anomalous difference map for the entire monomer is shown (orange map – contoured at 5.0 sigma), but density is only apparent around a calcium ion located ~16Å from the bound phenazine. Density for the bound 1-OH-PHZ molecules was apparent in each of the three subunits. Only the active site of the A chain monomer is shown here. There is no apparent density to support the presence of additional cofactors or metal atoms. (**C**) Zoomed in view of the loop containing the coordinated calcium ion.

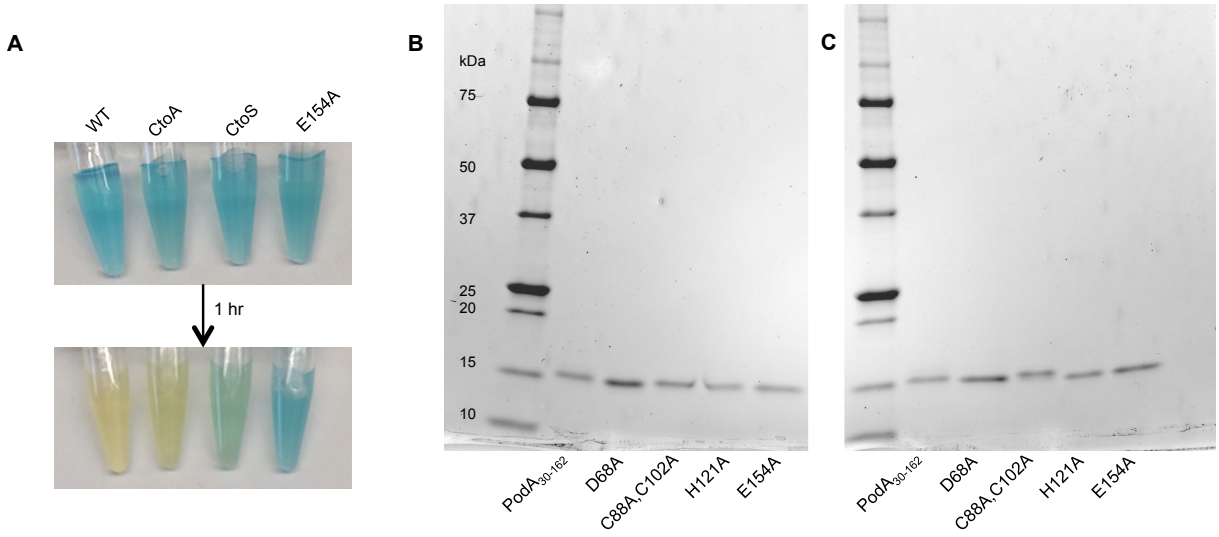

Fig. S6

(**A**) Both the C to A (C88A, C102A) and a C to S (C88S, C102S) double mutants show activity in cell-free lysates of *E. coli* BL21(DE3) expressing the protein of interest. While activity was always apparent in cell-free lysates, it was unstable and often lost upon further purification. (Note: the data for the C to A mutation in panels A-D of Figure 3 are from a rare preparation where protein remained active throughout purification.) C to S has less apparent activity than C to A, but serves as an independent confirmation of the phenotype. Cell lysates of the E154A mutant show that the loss of PYO is not due to an activity inherent to *E. coli*; furthermore, the accumulation of 1-OH-PHZ by both C to A and C to S lysates was confirmed by HPLC. (**B**) Reducing and (**C**) non-reducing SDS-PAGE of mutant $PodA_{30\text{-}162}$ proteins. Under reducing conditions, $PodA_{30\text{-}162}$ and mutant proteins all have similar migration through SDS-PAGE. Under non-reducing conditions, the presence of a disulfide bond leads to slightly faster migration through SDS-PAGE for all proteins except the C to A double mutant.

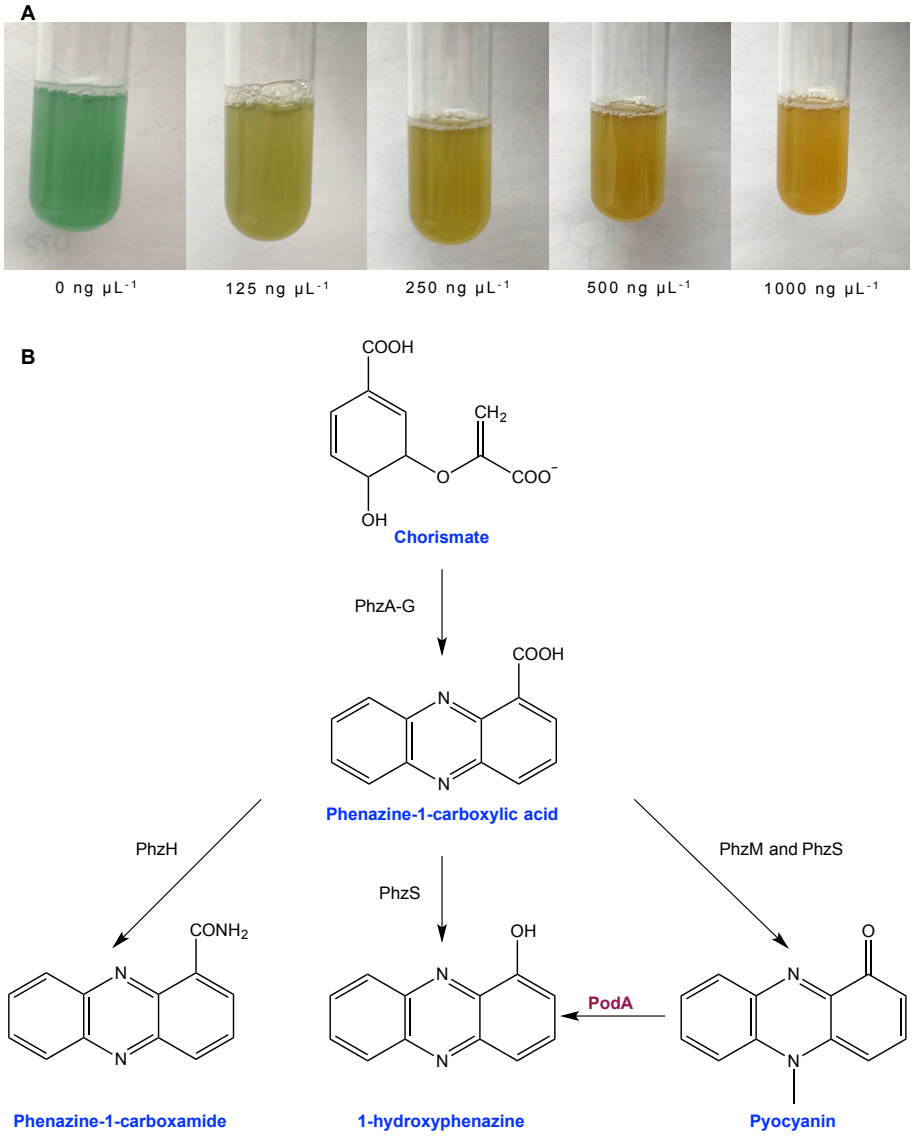

Fig. S7

(**A**) Dose dependence of $PodA_{30\text{-}162}$ activity in overnight cultures grown in TSB in the presence of the indicated amount of enzyme. Enzyme was added at the start of the culture and remained stable throughout the incubation period. (**B**) The phenazine biosynthetic pathways of *P. aeruginosa* (*40*). There is no known direct route for conversion of PYO or 1-OH-PHZ to PCA or PCN. Therefore, the response of *P. aeruginosa* to $PodA_{30\text{-}162}$ addition in Fig. S8 must be due to active regulatory control of the overall distribution of phenazines.

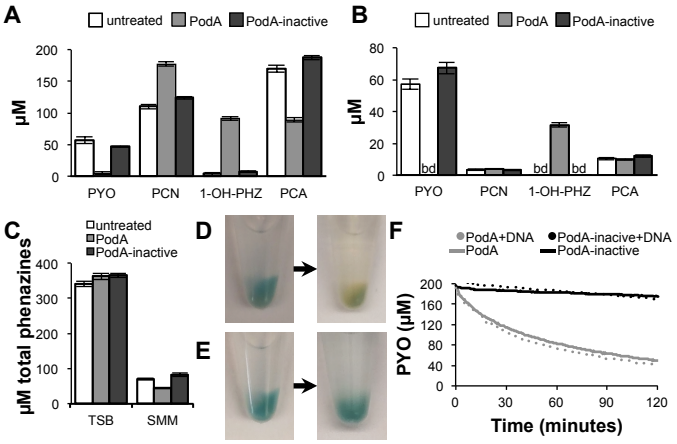

Fig. S8

$PodA_{30\text{-}162}$ alters phenazines in *P. aeruginosa* culture. $PodA_{30\text{-}162}$ alters phenazine concentrations in both TSB (**A**) and succinate minimal medium (SMM) (**B**). Data are averages from quadruplicate measurements and error bars represent one standard deviation around the mean. bd, below detection (< 0.5 µM). (**C**) Total phenazine concentrations in TSB and SSM as summed from panels A and B. While the distribution of phenazines is altered by $PodA_{30\text{-}162}$ in TSB, total concentrations remain constant. (**D**) PYO associated with precipitated DNA is not protected from $PodA_{30\text{-}162}$. (**E**) Inactivated $PodA_{30\text{-}162}$ does not demethylate PYO. (**F**) Solubilized DNA does not block $PodA_{30\text{-}162}$ activity. 200 µM PYO was incubated in the presence or absence of 400 µg mL^{-1} DNA (a stoichiometric excess). While these data do not preclude the possibility that PYO is loosely associated with DNA and may freely dissociate, and PodA may act on this solubilized PYO, they do confirm that DNA does not protect PYO from $PodA_{30\text{-}162}$ activity.

Table S1.

Data collection and refinement statistics for $PodA_{30-162}$

Space group	P21 21 21
Cell dimensions	
a, *b*, *c* (Å)	65.33, 72.98, 79.7
α, β, γ (°)	90, 90, 90
Resolution (Å)	34.98 - 1.8 (1.864 - 1.8)
R_{merge}	0.177 (1.98)
R_{meas}	0.180 (2.01)
R_{pim}	0.036 (0.391)
CC1/2	0.999 (0.827)
I/s(*I*)	13.3 (2.3)
Wilson B-factor	24.8
Completeness	1.00 (1.00)
Multiplicity	25.9 (26.1)
No. reflections used in refinement	35987 (3544)
R_{work} / R_{free}	0.168(0.271) / 0.195(0.283)
No. non-hydrogen atoms	2905
Macromolecules	2644
Ligands	48
Average *B* factor	36.5
Macromolecules	36.1
Ligands	36.4
Solvent	42.0
R.m.s. deviations	
Bond lengths (Å)	0.007
Bond angles (°)	0.94
Ramachandran plot statistics (%)	
Favored	98
Allowed	2.5
Outliers	0

Two crystals were used for data collection.
Values in parentheses are for highest-resolution shell.

Table S2.

Strains, primers and plasmids used in this study.

Strain	Reference
Pseudomonas aeruginosa PA14	(*32*)
P. aeruginosa Δphz	(*31*)
Escherichia coli BL21(DE3)	(*33*)

Plasmid	Description
pET20b(+)-*podA*$_{30\text{-}162}$	*podA*$_{30\text{-}162}$ expressed from the IPTG inducible promoter of pET-20b(+)
pET20b(+)-*podA*$_{30\text{-}162,\ D68A}$	D68A mutant *podA*$_{30\text{-}162}$ expressed from the IPTG inducible promoter of pET-20b(+)
pET20b(+)-*podA*$_{30\text{-}162,\ D72N}$	D72N mutant *podA*$_{30\text{-}162}$ expressed from the IPTG inducible promoter of pET-20b(+)
pET20b(+)-*podA*$_{30\text{-}162,\ C88A,C102A}$	C88A,C102A double mutant *podA*$_{30\text{-}162}$ expressed from the IPTG inducible promoter of pET-20b(+)
pET20b(+)-*podA*$_{30\text{-}162,\ C88S,C102S}$	C88S,C102S double mutant *podA*$_{30\text{-}162}$ expressed from the IPTG inducible promoter of pET-20b(+)
pET20b(+)-*podA*$_{30\text{-}162,\ H121A}$	H121A mutant *podA*$_{30\text{-}162}$ expressed from the IPTG inducible promoter of pET-20b(+)
pET20b(+)-*podA*$_{30\text{-}162,\ E154A}$	E154A mutant *podA*$_{30\text{-}162}$ expressed from the IPTG inducible promoter of pET-20b(+)
pET20b(+)-*podA*$_{30\text{-}162,\ Y156F}$	Y156F mutant *podA*$_{30\text{-}162}$ expressed from the IPTG inducible promoter of pET-20b(+)

Primer	Sequence
podA30-162-NdeI-F	AAAACATATGGACGGTCGCGGCGGCCGGAGTA
podA30-162-TEV-Pst-R	AAAACTGCAGTCAATGGTGATGGTGATGGTGGCTCTGGAAGTACAGGTTTTCGGCTTTCGTC AGTTTCAATTCGTACTTCTCA
podA30-162-pET20b-F-NdeI	AAAACATATGGACGGTCGCGGCGGCCGGAGTACA
podA30-162-pET20b-R-NotI	TTTTGCGGCCGCTCAATGGTGATGGTGATGGTGGCT
CtoS-F	GATAATCCAATGACCTATTCCGAACTGACCATTCACCTCGATGCAGGTGA
CtoS-R	CGGCGTCACATTGGTGAAAAAGGACGCGCCGCCGTCATATCCGACCTGCTTACCGT
CtoA-F	GGATAATCCAATGACCTATGCCGAACTGACCATTCACCTCGATGCAGGTGA
CtoA-R	GGCGTCACATTGGTGAAAAAGGCCGCGCCGCCGTCATATCCGACCTGCTTACCGTCT
D68A-F	GCCATCTTCTCCGACATCCTCTCGGTAGA
D68A-R	CATGTCTCCGACATCCATACCCGGT
H121A-F	GCCACACTCGCACCTTTCACCATGGCCA
H121A-R	CGGGGTGAGGCTACGGGCAAAGATCTCA
E154A-F	GCGAAGTACGAATTGAAACTGACGAAAGC
E154A-R	ATCGGGAGTCGCAACACCGGATACGGT

References and Notes

1. J. M. Turner, A. J. Messenger, Occurrence, biochemistry and physiology of phenazine pigment production. *Adv. Microb. Physiol.* **27**, 211–275 (1986). doi:10.1016/S0065-2911(08)60306-9 Medline

2. L. E. Dietrich, T. K. Teal, A. Price-Whelan, D. K. Newman, Redox-active antibiotics control gene expression and community behavior in divergent bacteria. *Science* **321**, 1203–1206 (2008). doi:10.1126/science.1160619 Medline

3. N. R. Glasser, S. E. Kern, D. K. Newman, Phenazine redox cycling enhances anaerobic survival in *Pseudomonas aeruginosa* by facilitating generation of ATP and a proton-motive force. *Mol. Microbiol.* **92**, 399–412 (2014). doi:10.1111/mmi.12566 Medline

4. A. Price-Whelan, L. E. Dietrich, D. K. Newman, Pyocyanin alters redox homeostasis and carbon flux through central metabolic pathways in *Pseudomonas aeruginosa* PA14. *J. Bacteriol.* **189**, 6372–6381 (2007). doi:10.1128/JB.00505-07 Medline

5. I. Ramos, L. E. Dietrich, A. Price-Whelan, D. K. Newman, Phenazines affect biofilm formation by *Pseudomonas aeruginosa* in similar ways at various scales. *Res. Microbiol.* **161**, 187–191 (2010). doi:10.1016/j.resmic.2010.01.003 Medline

6. Y. Wang, J. C. Wilks, T. Danhorn, I. Ramos, L. Croal, D. K. Newman, Phenazine-1-carboxylic acid promotes bacterial biofilm development via ferrous iron acquisition. *J. Bacteriol.* **193**, 3606–3617 (2011). doi:10.1128/JB.00396-11 Medline

7. W. J. Moree, V. V. Phelan, C.-H. Wu, N. Bandeira, D. S. Cornett, B. M. Duggan, P. C. Dorrestein, Interkingdom metabolic transformations captured by microbial imaging mass spectrometry. *Proc. Natl. Acad. Sci. U.S.A.* **109**, 13811–13816 (2012). doi:10.1073/pnas.1206855109 Medline

8. Z. J. Yang, W. Wang, Y. Jin, H.-B. Hu, X.-H. Zhang, Y.-Q. Xu, Isolation, identification, and degradation characteristics of phenazine-1-carboxylic acid-degrading strain *Sphingomonas* sp. DP58. *Curr. Microbiol.* **55**, 284–287 (2007). doi:10.1007/s00284-006-0522-7 Medline

9. K. C. Costa, M. Bergkessel, S. Saunders, J. Korlach, D. K. Newman, Enzymatic degradation of phenazines can generate energy and protect sensitive organisms from toxicity. *MBio* **6**, e01520–e15 (2015). doi:10.1128/mBio.01520-15 Medline

10. A. Krogh, B. Larsson, G. von Heijne, E. L. Sonnhammer, Predicting transmembrane protein topology with a hidden Markov model: Application to complete genomes. *J. Mol. Biol.* **305**, 567–580 (2001). doi:10.1006/jmbi.2000.4315 Medline

11. R. Anand, R. Marmorstein, Structure and mechanism of lysine-specific demethylase enzymes. *J. Biol. Chem.* **282**, 35425–35429 (2007). doi:10.1074/jbc.R700027200 Medline

12. J. M. Hagel, P. J. Facchini, Biochemistry and occurrence of O-demethylation in plant metabolism. *Front. Physiol.* **1**, 14 (2010). doi:10.3389/fphys.2010.00014 Medline

13. R. M. Summers, T. M. Louie, C.-L. Yu, L. Gakhar, K. C. Louie, M. Subramanian, Novel, highly specific N-demethylases enable bacteria to live on caffeine and related purine alkaloids. *J. Bacteriol.* **194**, 2041–2049 (2012). doi:10.1128/JB.06637-11 Medline

14. Y. Song, F. DiMaio, R. Y.-R. Wang, D. Kim, C. Miles, T. Brunette, J. Thompson, D. Baker, High-resolution comparative modeling with RosettaCM. *Structure* **21**, 1735–1742 (2013). doi:10.1016/j.str.2013.08.005 Medline

15. S. Raman, R. Vernon, J. Thompson, M. Tyka, R. Sadreyev, J. Pei, D. Kim, E. Kellogg, F. DiMaio, O. Lange, L. Kinch, W. Sheffler, B.-H. Kim, R. Das, N. V. Grishin, D. Baker, Structure prediction for CASP8 with all-atom refinement using Rosetta. *Proteins* **77** (Suppl 9), 89–99 (2009). doi:10.1002/prot.22540 Medline

16. D. E. Kim, D. Chivian, D. Baker, Protein structure prediction and analysis using the Robetta server. *Nucleic Acids Res.* **32** (Web Server), W526–W531 (2004). doi:10.1093/nar/gkh468 Medline

17. A. Gutteridge, J. M. Thornton, Understanding nature's catalytic toolkit. *Trends Biochem. Sci.* **30**, 622–629 (2005). doi:10.1016/j.tibs.2005.09.006 Medline

18. C. T. Walsh, T. A. Wencewicz, Flavoenzymes: Versatile catalysts in biosynthetic pathways. *Nat. Prod. Rep.* **30**, 175–200 (2013). doi:10.1039/C2NP20069D Medline

19. C. B. Whitchurch, T. Tolker-Nielsen, P. C. Ragas, J. S. Mattick, Extracellular DNA required for bacterial biofilm formation. *Science* **295**, 1487 (2002). doi:10.1126/science.295.5559.1487 Medline

20. T. Das, M. Manefield, Pyocyanin promotes extracellular DNA release in *Pseudomonas aeruginosa*. *PLOS ONE* **7**, e46718 (2012). doi:10.1371/journal.pone.0046718 Medline

21. T. Das, M. Manefield, Phenazine production enhances extracellular DNA release via hydrogen peroxide generation in *Pseudomonas aeruginosa*. *Commun. Integr. Biol.* **6**, e23570 (2013). doi:10.4161/cib.23570 Medline

22. T. Das, S. K. Kutty, R. Tavallaie, A. I. Ibugo, J. Panchompoo, S. Sehar, L. Aldous, A. W. S. Yeung, S. R. Thomas, N. Kumar, J. J. Gooding, M. Manefield, Phenazine virulence factor binding to extracellular DNA is important for *Pseudomonas aeruginosa* biofilm formation. *Sci. Rep.* **5**, 8398 (2015). doi:10.1038/srep08398 Medline

23. L. E. Dietrich, C. Okegbe, A. Price-Whelan, H. Sakhtah, R. C. Hunter, D. K. Newman, Bacterial community morphogenesis is intimately linked to the intracellular redox state. *J. Bacteriol.* **195**, 1371–1380 (2013). doi:10.1128/JB.02273-12 Medline

24. G. Borriello, E. Werner, F. Roe, A. M. Kim, G. D. Ehrlich, P. S. Stewart, Oxygen limitation contributes to antibiotic tolerance of *Pseudomonas aeruginosa* in biofilms. *Antimicrob. Agents Chemother.* **48**, 2659–2664 (2004). doi:10.1128/AAC.48.7.2659-2664.2004 Medline

25. Y. Wang, S. E. Kern, D. K. Newman, Endogenous phenazine antibiotics promote anaerobic survival of *Pseudomonas aeruginosa* via extracellular electron transfer. *J. Bacteriol.* **192**, 365–369 (2010). doi:10.1128/JB.01188-09 Medline

26. Y. Wang, D. K. Newman, Redox reactions of phenazine antibiotics with ferric (hydr)oxides and molecular oxygen. *Environ. Sci. Technol.* **42**, 2380–2386 (2008). doi:10.1021/es702290a Medline

27. T. Bjarnsholt, M. Alhede, M. Alhede, S. R. Eickhardt-Sørensen, C. Moser, M. Kühl, P. Ø. Jensen, N. Høiby, The in vivo biofilm. *Trends Microbiol.* **21**, 466–474 (2013). doi:10.1016/j.tim.2013.06.002 Medline

28. K. N. Kragh, J. B. Hutchison, G. Melaugh, C. Rodesney, A. E. L. Roberts, Y. Irie, P. Ø. Jensen, S. P. Diggle, R. J. Allen, V. Gordon, T. Bjarnsholt, Role of multicellular aggregates in biofilm formation. *MBio* **7**, e00237-16 (2016). doi:10.1128/mBio.00237-16 Medline

29. E. S. Cowley, S. H. Kopf, A. LaRiviere, W. Ziebis, D. K. Newman, Pediatric cystic fibrosis sputum can be chemically dynamic, anoxic, and extremely reduced due to hydrogen sulfide formation. *MBio* **6**, e00767-15 (2015). doi:10.1128/mBio.00767-15 Medline

30. M. E. Taga, N. A. Larsen, A. R. Howard-Jones, C. T. Walsh, G. C. Walker, BluB cannibalizes flavin to form the lower ligand of vitamin B12. *Nature* **446**, 449–453 (2007). doi:10.1038/nature05611 Medline

31. L. E. Dietrich, A. Price-Whelan, A. Petersen, M. Whiteley, D. K. Newman, The phenazine pyocyanin is a terminal signalling factor in the quorum sensing network of *Pseudomonas aeruginosa*. *Mol. Microbiol.* **61**, 1308–1321 (2006). doi:10.1111/j.1365-2958.2006.05306.x Medline

32. L. G. Rahme, E. J. Stevens, S. F. Wolfort, J. Shao, R. G. Tompkins, F. M. Ausubel, Common virulence factors for bacterial pathogenicity in plants and animals. *Science* **268**, 1899–1902 (1995). doi:10.1126/science.7604262 Medline

33. F. W. Studier, B. A. Moffatt, Use of bacteriophage T7 RNA polymerase to direct selective high-level expression of cloned genes. *J. Mol. Biol.* **189**, 113–130 (1986). doi:10.1016/0022-2836(86)90385-2 Medline

34. S. K. DasGupta, S. Jain, D. Kaushal, A. K. Tyagi, Expression systems for study of mycobacterial gene regulation and development of recombinant BCG vaccines. *Biochem. Biophys. Res. Commun.* **246**, 797–804 (1998). doi:10.1006/bbrc.1998.8724 Medline

35. Y. P. Shih, H. C. Wu, S. M. Hu, T. F. Wang, A. H. Wang, Self-cleavage of fusion protein in vivo using TEV protease to yield native protein. *Protein Sci.* **14**, 936–941 (2005). doi:10.1110/ps.041129605 Medline

36. M. M. Bradford, A rapid and sensitive method for the quantitation of microgram quantities of protein utilizing the principle of protein-dye binding. *Anal. Biochem.* **72**, 248–254 (1976). doi:10.1016/0003-2697(76)90527-3 Medline

37. T. Nash, The colorimetric estimation of formaldehyde by means of the Hantzsch reaction. *Biochem. J.* **55**, 416–421 (1953). doi:10.1042/bj0550416 Medline

38. S. B. Jones, C. M. Terry, T. E. Lister, D. C. Johnson, Determination of submicromolar concentrations of formaldehyde by liquid chromatography. *Anal. Chem.* **71**, 4030–4033 (1999). doi:10.1021/ac990266s

39. N. L. Sullivan, D. S. Tzeranis, Y. Wang, P. T. So, D. Newman, Quantifying the dynamics of bacterial secondary metabolites by spectral multiphoton microscopy. *ACS Chem. Biol.* **6**, 893–899 (2011). doi:10.1021/cb200094w Medline

40. D. V. Mavrodi, R. F. Bonsall, S. M. Delaney, M. J. Soule, G. Phillips, L. S. Thomashow, Functional analysis of genes for biosynthesis of pyocyanin and phenazine-1-carboxamide from *Pseudomonas aeruginosa* PAO1. *J. Bacteriol.* **183**, 6454–6465 (2001). doi:10.1128/JB.183.21.6454-6465.2001 Medline

41. G. Kemmer, S. Keller, Nonlinear least-squares data fitting in Excel spreadsheets. *Nat. Protoc.* **5**, 267–281 (2010). doi:10.1038/nprot.2009.182 Medline

42. H. McIlwain, The phenazine series. Part IV. Reactionsof alkyl phenazonium salts; the phenazyls. *J. Chem. Soc.* 1704–1711 (1937). doi:10.1039/jr9370001704

43. W. Kabsch, Xds. *Acta Crystallogr. D Biol. Crystallogr.* **66**, 125–132 (2010). doi:10.1107/S0907444909047337 Medline

44. W. Kabsch, Integration, scaling, space-group assignment and post-refinement. *Acta Crystallogr. D Biol. Crystallogr.* **66**, 133–144 (2010). doi:10.1107/S0907444909047374 Medline

45. P. Evans, Scaling and assessment of data quality. *Acta Crystallogr. D Biol. Crystallogr.* **62**, 72–82 (2006). doi:10.1107/S0907444905036693 Medline

46. P. R. Evans, G. N. Murshudov, How good are my data and what is the resolution? *Acta Crystallogr. D Biol. Crystallogr.* **69**, 1204–1214 (2013). doi:10.1107/S0907444913000061 Medline

47. J. E. Padilla, T. O. Yeates, A statistic for local intensity differences: Robustness to anisotropy and pseudo-centering and utility for detecting twinning. *Acta Crystallogr. D Biol. Crystallogr.* **59**, 1124–1130 (2003). doi:10.1107/S0907444903007947 Medline

48. M. D. Winn, C. C. Ballard, K. D. Cowtan, E. J. Dodson, P. Emsley, P. R. Evans, R. M. Keegan, E. B. Krissinel, A. G. W. Leslie, A. McCoy, S. J. McNicholas, G. N. Murshudov, N. S. Pannu, E. A. Potterton, H. R. Powell, R. J. Read, A. Vagin, K. S. Wilson, Overview of the CCP4 suite and current developments. *Acta Crystallogr. D Biol. Crystallogr.* **67**, 235–242 (2011). doi:10.1107/S0907444910045749 Medline

49. A. J. McCoy, R. W. Grosse-Kunstleve, P. D. Adams, M. D. Winn, L. C. Storoni, R. J. Read, Phaser crystallographic software. *J. Appl. Crystallogr.* **40**, 658–674 (2007). doi:10.1107/S0021889807021206 Medline

50. P. Emsley, B. Lohkamp, W. G. Scott, K. Cowtan, Features and development of Coot. *Acta Crystallogr. D Biol. Crystallogr.* **66**, 486–501 (2010). doi:10.1107/S0907444910007493 Medline

51. T. C. Terwilliger, R. W. Grosse-Kunstleve, P. V. Afonine, N. W. Moriarty, P. H. Zwart, L.-W. Hung, R. J. Read, P. D. Adams, Iterative model building, structure refinement and density modification with the PHENIX AutoBuild wizard. *Acta Crystallogr. D Biol. Crystallogr.* **D64**, 61–69 (2008). doi:10.1107/S090744490705024X Medline

52. J. J. Headd, N. Echols, P. V. Afonine, R. W. Grosse-Kunstleve, V. B. Chen, N. W. Moriarty, D. C. Richardson, J. S. Richardson, P. D. Adams, Use of knowledge-based restraints in phenix.refine to improve macromolecular refinement at low resolution. *Acta Crystallogr. D Biol. Crystallogr.* **68**, 381–390 (2012). doi:10.1107/S0907444911047834 Medline

53. P. V. Afonine, R. W. Grosse-Kunstleve, N. Echols, J. J. Headd, N. W. Moriarty, M. Mustyakimov, T. C. Terwilliger, A. Urzhumtsev, P. H. Zwart, P. D. Adams, Towards automated crystallographic structure refinement with phenix.refine. *Acta Crystallogr. D Biol. Crystallogr.* **68**, 352–367 (2012). doi:10.1107/S0907444912001308 Medline

54. T. C. Terwilliger, P. D. Adams, N. W. Moriarty, J. D. Cohn, Ligand identification using electron-density map correlations. *Acta Crystallogr. D Biol. Crystallogr.* **63**, 101–107 (2007). doi:10.1107/S0907444906046233 Medline

55. T. C. Terwilliger, H. Klei, P. D. Adams, N. W. Moriarty, J. D. Cohn, Automated ligand fitting by core-fragment fitting and extension into density. *Acta Crystallogr. D Biol. Crystallogr.* **62**, 915–922 (2006). doi:10.1107/S0907444906017161 Medline

56. P. D. Adams, P. V. Afonine, G. Bunkóczi, V. B. Chen, I. W. Davis, N. Echols, J. J. Headd, L.-W. Hung, G. J. Kapral, R. W. Grosse-Kunstleve, A. J. McCoy, N. W. Moriarty, R. Oeffner, R. J. Read, D. C. Richardson, J. S. Richardson, T. C. Terwilliger, P. H. Zwart, PHENIX: A comprehensive Python-based system for macromolecular structure solution. *Acta Crystallogr. D Biol. Crystallogr.* **66**, 213–221 (2010). doi:10.1107/S0907444909052925 Medline

57. N. W. Moriarty, R. W. Grosse-Kunstleve, P. D. Adams, electronic Ligand Builder and Optimization Workbench (eLBOW): A tool for ligand coordinate and restraint generation. *Acta Crystallogr. D Biol. Crystallogr.* **65**, 1074–1080 (2009). doi:10.1107/S0907444909029436 Medline

58. M. D. Winn, M. N. Isupov, G. N. Murshudov, Use of TLS parameters to model anisotropic displacements in macromolecular refinement. *Acta Crystallogr. D Biol. Crystallogr.* **57**, 122–133 (2001). doi:10.1107/S0907444900014736 Medline

59. T. Das, S. K. Kutty, N. Kumar, M. Manefield, Pyocyanin facilitates extracellular DNA binding to *Pseudomonas aeruginosa* influencing cell surface properties and aggregation. *PLOS ONE* **8**, e58299 (2013). doi:10.1371/journal.pone.0058299 Medline

60. C. A. Schneider, W. S. Rasband, K. W. Eliceiri, NIH Image to ImageJ: 25 years of image analysis. *Nat. Methods* **9**, 671–675 (2012). doi:10.1038/nmeth.2089 Medline

61. S. Bolte, F. P. Cordelières, A guided tour into subcellular colocalization analysis in light microscopy. *J. Microsc.* **224**, 213–232 (2006). doi:10.1111/j.1365-2818.2006.01706.x Medline

62. D. Cohen, U. Mechold, H. Nevenzal, Y. Yarmiyhu, T. E. Randall, D. C. Bay, J. D. Rich, M. R. Parsek, V. Kaever, J. J. Harrison, E. Banin, Oligoribonuclease is a central feature of cyclic diguanylate signaling in *Pseudomonas aeruginosa*. *Proc. Natl. Acad. Sci. U.S.A.* **112**, 11359–11364 (2015). doi:10.1073/pnas.1421450112 Medline